ADVANCES IN ATMOSPHERIC SCIENCES, VOL. 33, AUGUST 2016, 945–954

Determination of the Effect of Initial Inner-Core Structure on Tropical Cyclone Intensification and Track on a Beta Plane

Guanghua CHEN*

Center for Monsoon System Research, Institute of Atmospheric Physics, Chinese Academy of Sciences, Beijing 100190

(Received 14 November 2015; revised 26 March 2016; accepted 14 April 2016)

ABSTRACT

The sensitivity of TC intensification and track to the initial inner-core structure on a β plane is investigated using a numerical model. The results show that the vortex with large inner-core winds (CVEX-EXP) experiences an earlier intensification than that with small inner-core winds (CCAVE-EXP), but they have nearly the same intensification rate after spin-up. In the early stage, the convective cells associated with surface heat flux are mainly confined within the inner-core region in CVEX-EXP, whereas the vortex in CCAVE-EXP exhibits a considerably asymmetric structure with most of the convective vortices being initiated to the northeast in the outer-core region due to the β effect. The large inner-core inertial stability in CVEX-EXP can prompt a high efficiency in the conversion from convective heating to kinetic energy. In addition, much stronger straining deformation and PBL imbalance in the inner-core region outside the primary eyewall ensue during the initial development stage in CVEX-EXP than in CCAVE-EXP, which is conducive to the rapid axisymmetrization and early intensification in CVEX-EXP. The TC track in CVEX-EXP sustains a northwestward displacement throughout the integration, whereas the TC in CCAVE-EXP undergoes a northeastward recurvature when the asymmetric structure is dominant. Due to the enhanced asymmetric convection to the northeast of the TC center in CCAVE-EXP, a pair of secondary gyres embedded within the large-scale primary β gyres forms, which modulates the ventilation flow and thus steers the TC to move northeastward.

Key words: inner-core structure, tropical cyclone, intensification, track, β plane

Citation: Chen, G. H., 2016: Determination of the effect of initial inner-core structure on tropical cyclone intensification and track on a beta plane. *Adv. Atmos. Sci.*, **33**(8), 945–954, doi: 10.1007/s00376-016-5241-9.

1. Introduction

The prediction of tropical cyclone (TC) intensity change is a very challenging task, because it involves complex physics during TC evolution. A considerable body of research has been conducted to reveal the impacts on TC intensity change from multiscale interactions of different phenomena, such as sea surface temperature, vertical wind shear, environmental moisture, and cloud microphysics (e.g., DeMaria, 1996; Emanuel et al., 2004; Zhu and Zhang, 2006). Although there have been some improvements in TC intensity forecasting in recent years (Rappaport et al., 2009), our understanding and prediction of TC intensification remains limited.

Previous studies have revealed TC intensity variation on different planes in the absence of environmental flows. For instance, Li et al. (2012) elucidated the dependence of TC intensification on the Coriolis parameter. They reported that faster TC intensification in a lower planetary vorticity environment than a higher planetary vorticity environment can be attributed to the boundary layer imbalance in relation with the earth planetary vorticity f. Madala and Piacsek (1975) documented that a vortex on a β plane intensified at a slower rate than the one on an f plane before the storm stage, but at the same rate thereafter. This discrepancy in TC development arises from a larger inertial stability in the upper layer and the vertical shearing of centers in a β-plane simulation (DeMaria and Schubert, 1984). In addition, the β-induced flow pattern generates asymmetric moisture convergence and surface fluxes, and a phase shift between their maxima, which can inhibit TC development (Peng et al., 1999; Wu and Braun, 2004). Recently, Ge et al. (2015) examined the influence of different inner-core structures on TC intensification on an f plane. They found that a vortex with a larger inner-core relative vorticity and inertial stability has a greater potential for conversion from diabatic heating to kinetic energy and small-scale convective vorticity aggregation, in contrast to that with a small inner-core vorticity and inertial stability. However, the role of the β effect in modulating TC structural evolution and intensification is not well understood, given distinct initial inner-core structures.

On the other hand, a substantial amount of TC research has been devoted to improving our understanding of TC movement. To a large degree, TC movement results mainly from the advection of TC relative vorticity by the environmental steering flow. However, when the steering flow is

* Corresponding author: Guanghua CHEN
Email: cgh@mail.iap.ac.cn

weak, the β effect due to the latitudinal variation of the Coriolis force causes the TC track to deviate from that specified by steering flow. An initially symmetric vortex will develop a pair of counter-rotating β gyres due to Rossby wave dispersion. In a barotropic framework, Chan and Williams (1987) demonstrated that if only the β effect is retained, without any feedback to vortex flow, the vortex would only be stretched to the west, without any significant displacement. Only through the inclusion of the nonlinear term can the vortex move towards the northwest, and this northwestward movement increases with both the maximum wind speed and the radius of maximum wind (RMW). Fiorino and Elsberry (1989) decomposed the flow into an axisymmetric and an asymmetric component, and showed that the β effect first causes the development of asymmetric vorticity, which is then rotated by the symmetric vortex flow, forming a southwest–northeast-oriented asymmetric streamfunction after an initial adjustment. As a result, the asymmetric flow associated with the gradient of streamfunction can advect the vortex vorticity towards the northwest. For a baroclinic vortex, because the tangential wind decreases with height, the intensity of β gyres and the associated ventilation flow will decrease with height. Therefore, the so-called differential β effect in the vertical direction plays an important role in vortex movement (Wang and Holland, 1996a). Besides, the existence of vertical shear and diabetic heating in the TC core can produce large-scale anticyclonic circulation and an associated PV anomaly in the upper-tropospheric outflow layer, which can then affect the lower level vortex motion through the vertical penetration flow (Wu and Emanuel, 1993; Wang and Holland, 1996b). Although some studies have stated that TC motion is insensitive to the wind structure in the inner region in a barotropic framework (e.g. Holland, 1983; DeMaria, 1985), the question regarding how different inner-core structures of a baroclinic vortex in a full-physics model modulate the β effect and cause the discrepancy in TC displacement needs to be further addressed.

The objective of this study is to examine the role of initial inner-core structure in TC intensification and track on a β plane. Section 2 presents the model configuration and experimental design. The effect of the inner-core structure on TC intensification is presented in section 3. Section 4 introduces the contribution of different inner-core structures to TC track. A summary is given in section 5.

2. Model configuration and experimental design

The WRF model, version 3.6, is adopted to investigate the sensitivity of TC intensification and track to the initial inner-core structure on a β plane. The environmental thermodynamic profiles are specified as the mean climatology in the TC peak region (5°–20°N, 130°–170°E) during July–September from 1979 to 2012, based on the Japanese 55-year Reanalysis (Ebita et al., 2011). The simulations are initialized with an axisymmetric vortex on a β plane centered at 18°N, with a variable Coriolis parameter, $f = f_0 + \beta y$ in which f_0 denotes the planetary vorticity at 18°N. The vortex is embedded in a quiescent environment over the ocean with a constant sea surface temperature of 29°C. The model contains three domains all with 271×271 grid points and with horizontal grid spacing of 27, 9 and 3 km, respectively. The innermost domain is designed to move with the model TC center.

The physics parameterizations include the WSM6 scheme (Hong et al., 2004), the YSU (Yonsei University) PBL scheme (Noh et al., 2003), the Dudhia shortwave parameterization (Dudhia, 1989), and the RRTM longwave parameterization (Mlawer et al., 1997). Considering that the domains are large enough to cover the convection in the inner-core area and outer spiral rainbands, cumulus parameterization is not adopted in the two innermost meshes in this study. The TC center is defined as the center of axisymmetric circulation along which the azimuthal mean wind at the lowest model level reaches the maximum at a given time.

Axisymmetric baroclinic vortices, with the same tangential wind profile outside the RMW but different ones inside the RMW, are superimposed on the horizontally uniform environment. Two idealized experiments are carried out with the model lowest-level tangential wind profile $V(r)$ beyond the RMW, defined by

$$V(r)=V_{\mathrm{m}}\left(\frac{r}{r_{\mathrm{m}}}\right)\left[\exp\left(1-\frac{r}{r_{\mathrm{m}}}\right)-\frac{|r-r_{\mathrm{m}}|}{R_0-r_{\mathrm{m}}}\exp\left(1-\frac{R_0}{r_{\mathrm{m}}}\right)\right], \quad r \geqslant r_{\mathrm{m}}, \tag{1}$$

where $V_{\mathrm{m}} = 12$ m s^{-1} is the maximum tangential wind at the RMW, $r_{\mathrm{m}} = 108$ km, r is the radius, and $R_0 = 900$ km is the radius at which the vortex wind vanishes. To discriminate the inner-core wind fields, the tangential wind profiles inside the RMW are specified as follows:

$$V_{\mathrm{m}}\left(\frac{r}{r_{\mathrm{m}}}\right)\exp\left(1-\frac{r}{r_{\mathrm{m}}}\right), \quad r < r_{\mathrm{m}}, \tag{2}$$

$$V_{\mathrm{m}}\left(\frac{r}{r_{\mathrm{m}}}\right)^3\exp\left(1-\frac{r}{r_{\mathrm{m}}}\right), \quad r < r_{\mathrm{m}}, \tag{3}$$

which denote the convex- and concave-shaped wind profiles within the RWM (Fig. 1a), corresponding to two experiments referred to as CVEX-EXP and CCAVE-EXP, respectively. In the vertical direction, the initial tangential wind profiles decrease sinusoidally with pressure to vanish at 100 hPa. The mass and thermodynamic fields associated with the vortex are obtained by solving the nonlinear balance equation (Wang, 1995).

3. Effect of the inner-core structure on TC intensification

Figure 2 exhibits the temporal evolution of TC intensity in terms of the minimum surface level pressure and maximum azimuthal mean wind speed at the lowest model level. The striking feature is that the TCs in the two experiments display distinct rapid intensification timings. Specifically, the vortex in CVEX-EXP commences intensification at 30 h of

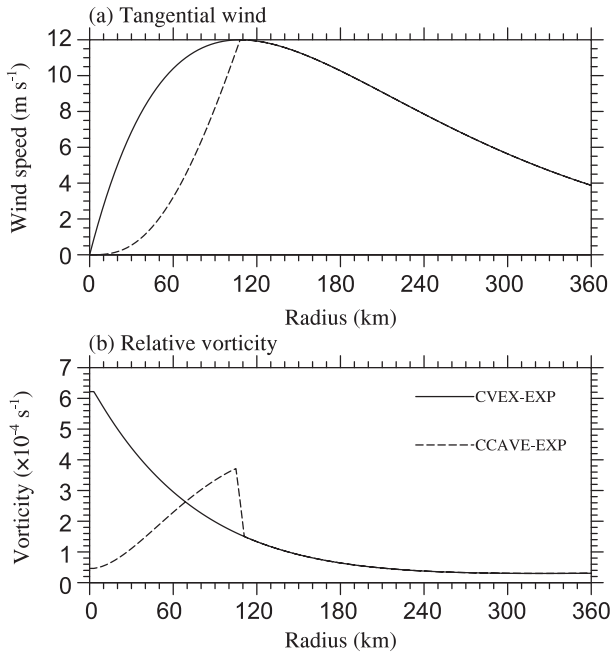

Fig. 1. Radial profiles of (a) tangential wind (units: m s^{-1}) and (b) relative vorticity (units: $\times 10^{-4}$ s^{-1}) at the lowest model level of the initial vortex in CVEX-EXP (solid line) and CCAVE-EXP (dashed line).

integration, while the rapid intensification of the storm in CCAVE-EXP starts at approximately 50 h. In the mature stage, the TCs in CVEX-EXP and CCAVE-EXP reach 928 hPa and 939 hPa at 84 h and 102 h, respectively. After that time, both of the TCs basically sustain their quasi-steady intensity, although the subsequent intensity seems to be oscillatory (Fig. 2a). The sensitivity of TC intensification to the initial inner-core structure is in agreement with the finding on an f plane in Ge et al. (2015), who showed the delayed intensification of a vortex with a Rankine-type structure, as compared to one with a convex-shaped structure, in the inner-core region.

The sharp contrast in TC intensification can be easily inferred from the radar reflectivity at the lowest model level. In the early stage of 24 h, sporadic small-scale convective vortices emerge within a radius of 60 km in CVEX-EXP (Fig. 3a), while sparse convective cells are scattered outside 60 km in CCAVE-EXP (Fig. 3g). As time proceeds, the convective systems in CVEX-EXP begin to grow through the merger of small-scale vortices and are organized around the TC center in the inner-core region (Fig. 3b). In contrast, although the vortex in CCAVE-EXP lacks convective cells inside 60 km, the loosely organized convective vortices mainly spread from eastern to northern sections of the outer-core region (Fig. 3h). Until 48 h of simulation, the convective systems in CVEX-EXP are well-organized, such that the convective ring shrinks inward forming a clear eye region (Fig. 3c). Whereas, the vortex in CCAVE-EXP undergoes a slower development with substantial convective activity in the northeastern semicircle in the absence of an eye (Fig. 3i). During the subsequent simulation, the vortex in CVEX-EXP contracts tightly, developing a nearly axisymmetric convective eyewall with reduced outer spiral rainbands (Figs. 3d–f). By comparison, until the vortex in CCAVE-EXP develops a well-defined eye after 50 h (Fig. 3j), the storm begins to intensify rapidly. Different from the suppressed outer spiral rainbands in CVEX-EXP, the convective bands are filamented in the outer-core region, giving rise to active outer spiral rainbands and a relatively large inner-core size (Figs. 3j–l). The active spiral rainbands can block the boundary layer inflow, which converges the mass into the eyewall, thus dynamically decreasing the primary eyewall convection and weakening the TC. On the other hand, the convective overturning induced by spiral rainbands produces compensating subsidence that introduces low equivalent potential temperature air from the middle troposphere down to the inflow boundary layer, which can thermodynamically limit TC intensity. The hydrostatic adjustment associated with the net diabatic heating in the outer spiral rainband also causes a reduction in the pressure gradient across the eyewall, which can weaken TC intensity but increase the size of the TC inner core (e.g. Shapiro and Willoughby, 1982; Powell, 1990; Wang, 2009). Therefore, the TC in CCAVE-EXP, with active outer spiral rainbands, evolves into a relatively less intense vortex in the mature stage compared to that in CVEX-EXP, as shown in Fig. 2a.

As depicted above, two striking differences during the initial spin-up stage between the two experiments can be observed: one is the lack of convective vortices in the inner-core region in CCAVE-EXP, compared to in CVEX-EXP; and the other is a more asymmetric structure in CCAVE-EXP, with vigorous outer convective rainbands in the northeastern quadrant. The discrepancies can be partly accounted for by the surface heat flux and wind field associated with the initial inner-core structure and β-induced asymmetry. Figure 4 depicts the distribution of surface heat flux and the wind field, averaged between 36 and 48 h of simulation. Consistent with the distribution of radar reflectivity in Fig. 3, the TC center is tightly surrounded by large surface heat flux within a radius of 60 km, due to the strong inner-core surface wind in CVEX-EXP (Figs. 4a and c). In sharp contrast, the surface heat flux positively proportional to the magnitude of inner-core wind speed is considerably suppressed in the CCAVE-EXP inner-core region, resulting in a reduction of inner-core convection (Figs. 4b and d). On the other hand, the surface heat flux and wind speed in CCAVE-EXP are highly asymmetric, with a maximum region located to the northeast outside the inner core. This is in good agreement with the findings of Chan and Williams (1987), who identified that the β-effect and nonlinear effect combined can create a wind speed maximum to the northeast of the vortex and, moreover, the asymmetry in the outer-core region is more evident than in the inner-core region. Comparatively, although the wind speed in CVEX-EXP appears somewhat asymmetrically, the well-organized eyewall and maximum wind enclose the TC center almost axisymmetrically (Fig. 4c).

In addition to the wind-induced surface heat exchange (WISHE) emphasized above, two extra experiments are con-

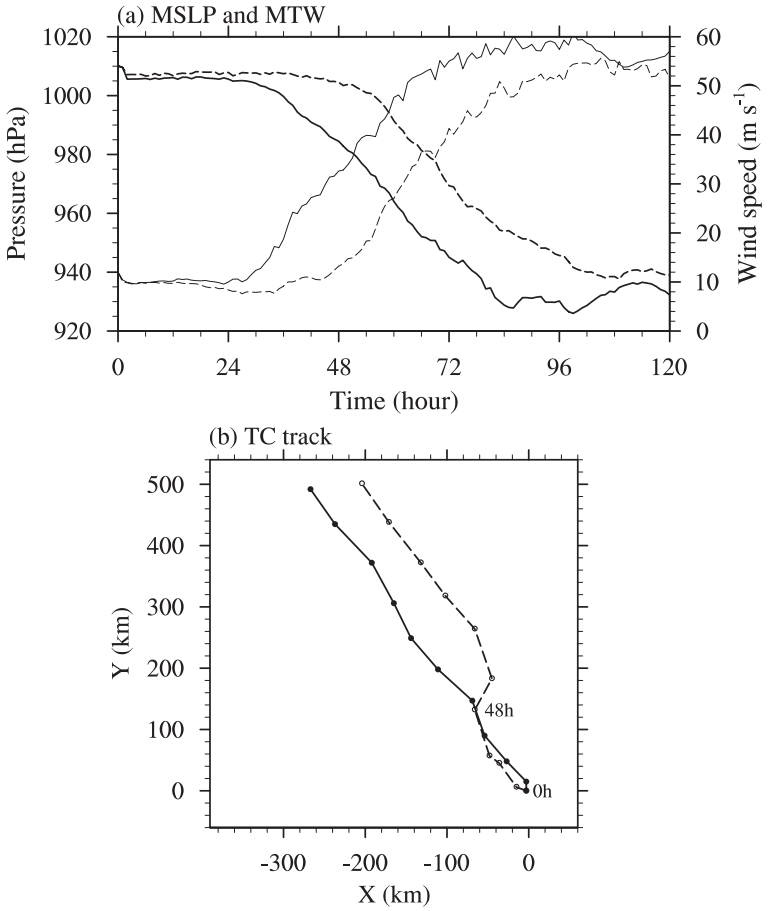

Fig. 2. Temporal evolution of the (a) minimum sea level pressure (units: hPa; thick line) and maximum azimuthal mean wind speed (units: m s^{-1}; thin line) at the lowest model level in CVEX-EXP (solid line) and CCAVE-EXP (dashed line), and (b) the TC track, with dots indicating the 12-h positions in CVEX-EXP (solid line) and CCAVE-EXP (dashed line).

ducted, in which the latent heat flux and sensible heat flux at the surface are fixed at 100 W m^{-2} and 20 W m^{-2}, respectively, throughout the integration, in such a way that the difference in vortex development can be further tested under the theory of conditional instability of the second kind (CISK). The results show that, given the same surface heat flux, the well-organized convective vortices in CVEX-EXP emerge to the northeast of the TC center, which is earlier than that in CCAVE-EXP. The vigorous convective vortices concentrate within a radius of 60 km in CVEX-EXP, while they are outside 60 km in CCAVE-EXP. In the absence of the WISHE mechanism, the extra experiments exhibit qualitatively similar results to those with WISHE involved, albeit with a relatively slow intensification rate due to the small magnitude of surface heat flux (not shown). It suggests that the CISK-type mechanism can also lead to the distinct vortex development given the different inner-core structure profiles. Besides, the convectively generated mesoscale positive vorticity anomalies tend to move up the ambient vorticity gradient (e.g., Schecter and Dubin, 1999; Ge et al., 2015). Figure 1b exhibits a salient difference in the initial profile of relative vorticity, in that the large vorticity magnitude and its negative radial gradient are within a radius of 70 km in CVEX-EXP (in contrast to those in CCAVE-EXP), which is favorable for vorticity aggregation and convergence, and subsequent formation of a self-amplified mesoscale core vortex. The stronger the inner-core background low-level vorticity, the greater the Ekman pumping effect and diabatic heating, and thus the earlier the TC intensification.

Another important dynamic parameter—the so-called effective β—can be used to measure the extent to which the spiral convective band is facilitated in the inner-core region. The effective β is defined as $(-\partial\bar{q}/\partial r)(\bar{\xi}/\bar{q})$, with $\bar{q}$ and $\bar{\xi} = f + 2\bar{V}_t/r$ denoting the azimuthal mean potential vorticity and modified Coriolis parameter, respectively, in which $\bar{V}_t$ denotes the azimuthally-mean tangential wind. Previous studies indicate that a well-defined low-level β skirt favor the formation of a well-organized spiral rainband outside the eyewall, via the maintenance of long-lasting deep convection and the upscale transfer of energy from convective-scale motion (e.g., Terwey and Montgomery, 2008; Fang and Zhang, 2012). In Fig. 5 we can see that the low-level effective β averaged from 36 to 48 h in CVEX-EXP is almost positive radially outward from 15 km, with a maximum at a radius of 27 km. There-

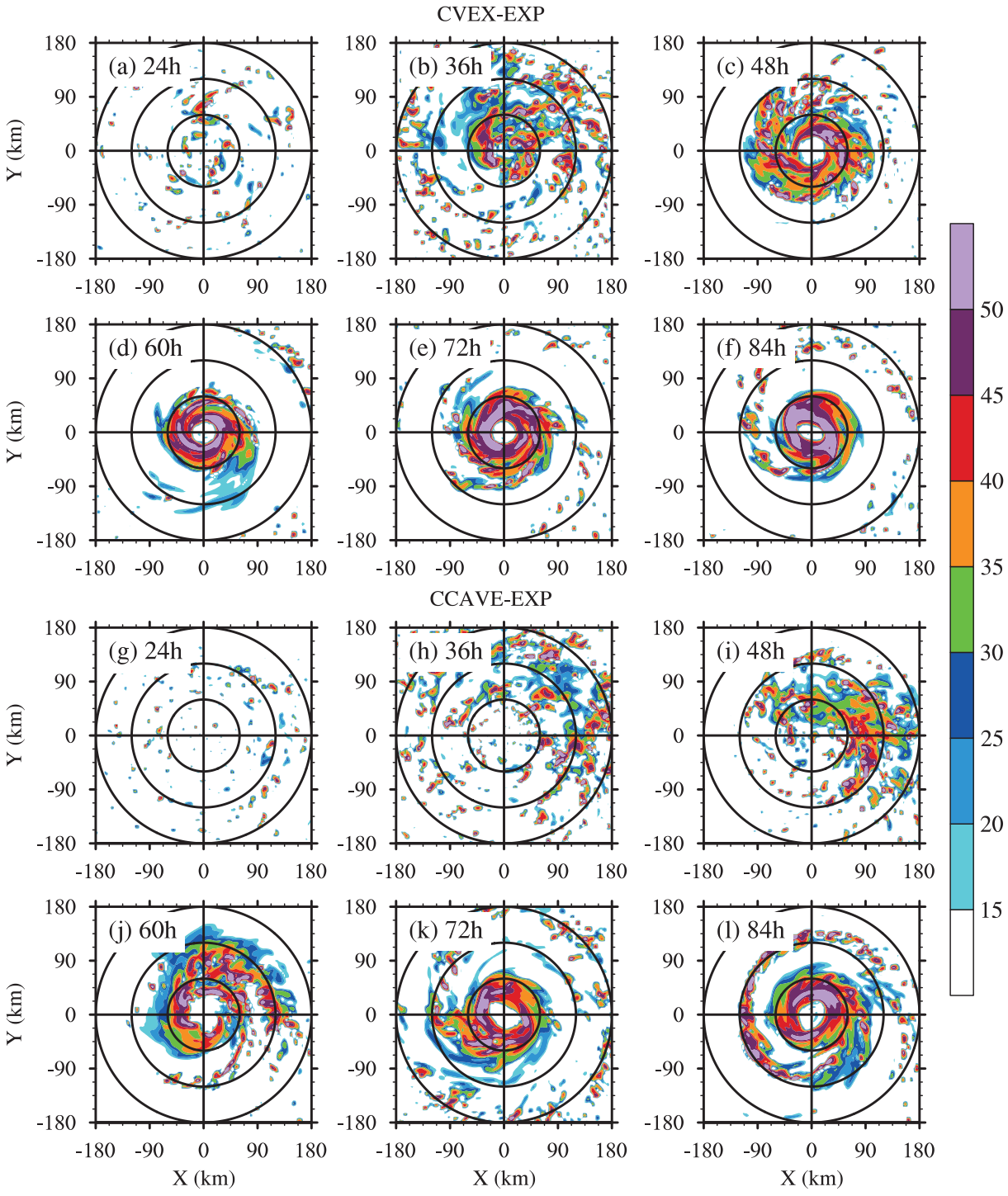

Fig. 3. Plan view of the 12-hourly simulated radar reflectivity (units: dBZ) at the height of 1 km, from 24 h to 84 h, in (a–f) CVEX-EXP and (g–l) CCAVE-EXP. The domain shown in each panel is 360 km × 360 km. The *x*-axis and *y*-axis denote the east–west and south–north distance, respectively.

fore, the β skirt outside of the eyewall is sufficient to constrain the asymmetric flow and prompt the transfer of perturbation vorticity and kinetic energy from sporadic deep convection to azimuthal mean flow, which in turn promotes the axisymmetrization of asymmetric eddies and rapid intensification in CVEX-EXP (Fig. 5a). In contrast, the positive effective β only occurs outside 60 km in CCAVE-EXP and, moreover, with much smaller magnitude, suggesting that CCAVE-EXP has an unfavorable inner-core dynamic condition that is hostile to the robust activity of an inner spiral rainband, and thus delays intensification (Fig. 5b).

The response of the secondary circulation to the heat source is sensitive to inertial stability, defined as $I = \sqrt{(f+2V/r)[f+\partial(rV)/r\partial r]}$. The vortex intensification be-

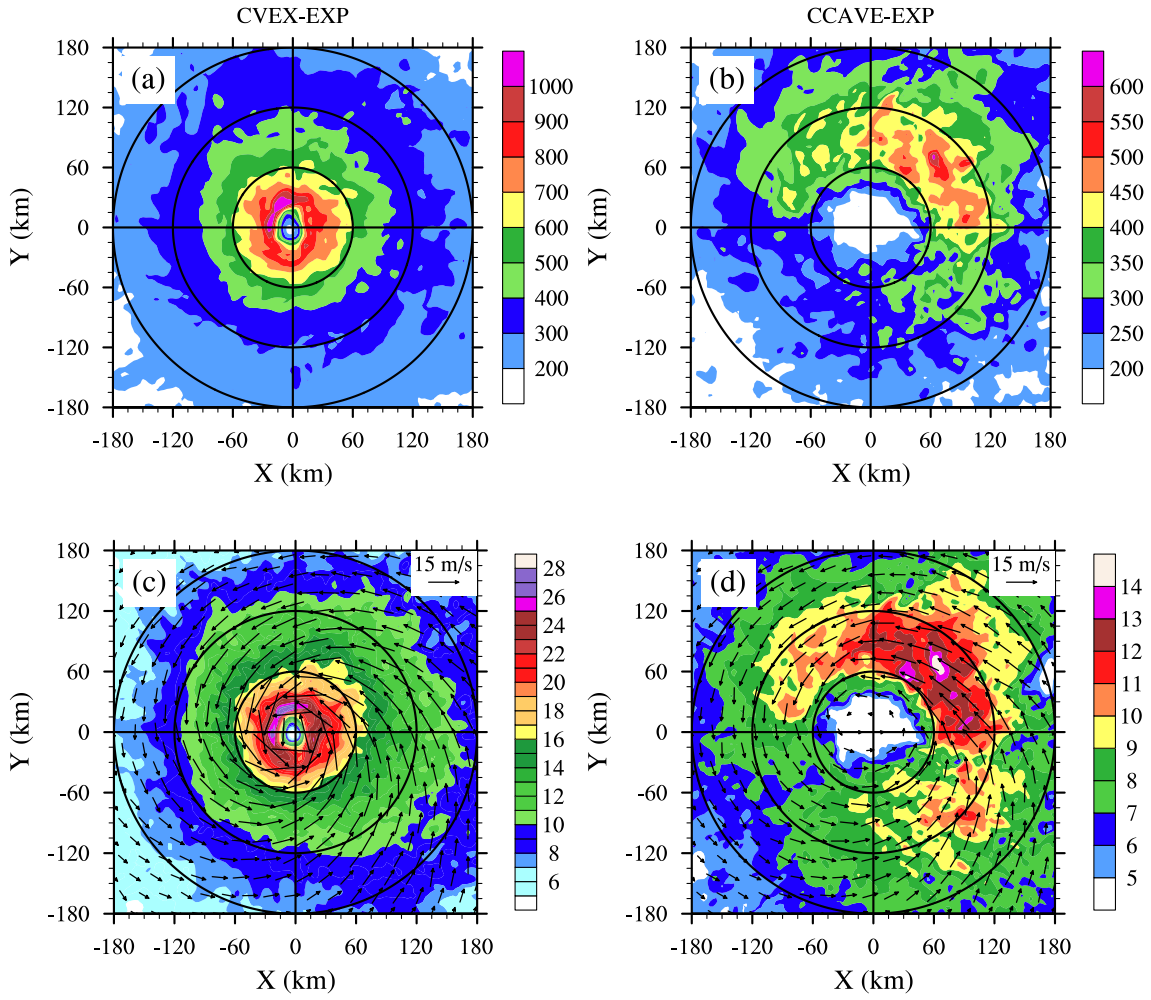

Fig. 4. The distribution of (a, b) surface heat flux (units: W m^{-2}) and (c, d) 10-m wind vector and speed (units: m s^{-1}), averaged between 36 and 48 h, in (a, c) CVEX-EXP and (b, d) CCAVE-EXP. The domain shown in each panel is 360 km × 360 km. The *x*-axis and *y*-axis denote the east–west and south–north distance, respectively.

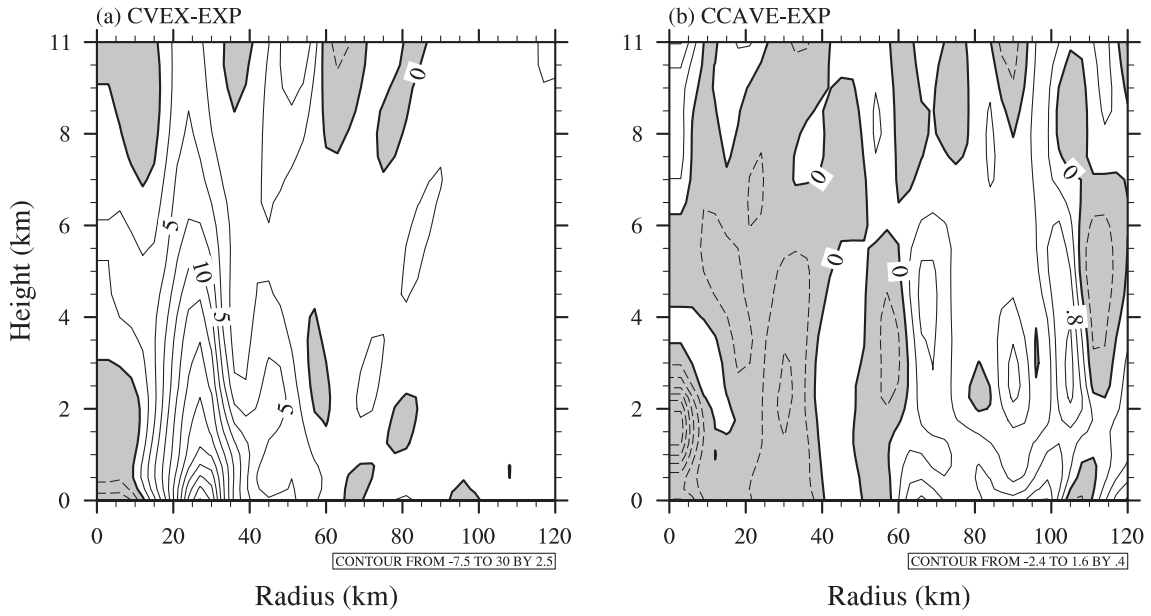

Fig. 5. Radius–height cross section of the azimuthal mean effective β (units: $\times 10^{-8}$ m^{-1} s^{-1}), averaged from 36 to 48 h, in (a) CVEX-EXP and (b) CCAVE-EXP. The regions with negative values are shaded.

comes more efficient for a given heat source with increasing inertial stability (e.g. Schubert and Hack, 1982; Shapiro and Willoughby, 1982; Hack and Schubert, 1986). When the inertial stability is high, internal atmospheric heating can effectively warm the atmospheric column and lower the surface pressure. Physically, a larger inertial stability corresponds to a smaller Rossby deformation radius, causing the energy produced by the diabatic heating to be confined within a smaller radius, rather than dispersed by gravity waves, as the inertial stability is low. Figure 6 clearly shows that the inertial stability inside 60 km is much larger in CVEX-EXP than in CCAVE-EXP, which implies an increase in efficiency with which the latent heating can locally warm the troposphere and increase the tangential winds. Comparatively, the inertial stability outside 90 km in CCAVE-EXP is slightly larger, which may be attributable to the relatively large winds in the outer-core region to the northeast, related to β-induced asymmetry, as shown in Fig. 4d.

Recent work has identified the role of the unbalanced PBL process in TC intensification (e.g., Bui et al., 2009; Huang et al., 2012). Bui et al. (2009) found that PBL balanced theory underestimates the low-level radial inflow, and therefore the maximum azimuthal-mean tangential wind tendency. The accelerated radial inflow associated with the PBL imbalanced process can enhance the inward advection of high absolute angular momentum, and thus increase vortex intensity. A useful way to quantify the unbalanced component of boundary layer dynamics is to compute the agradient force (AF), defined as the sum of the azimuthally averaged radial pressure gradient force, the Coriolis force, and centrifugal forces:

$$\mathrm{AF} = -\frac{1}{\rho}\frac{\partial \bar{p}}{\partial r} + f\bar{v} + \frac{\bar{v}^2}{r}\,, \tag{4}$$

where p is pressure, ρ is the air density, and v is the tangential wind. The overbar represents the azimuthal-mean component. AF < 0 (AF > 0) corresponds to the subgradient (supergradient) radial inflow, indicating a tendency to accelerate (decelerate) the inflows toward the vortex center. Figure 7 shows the agradient force averaged below 2 km from 24 to 48 h. It displays clearly that, in CVEX-EXP, the strong outward-directed (positive) agradient force resides within 36 km, with the maximum at 20 km, while the inward-directed (negative) agradient force exists outside the radius of 36 km. This radial profile of agradient force implies the convergence of radial flow appears in the zone with the decelerated flow on its radially inward side, and the accelerated flow on its radially outward side. The enhanced accelerated radial inflows on the radially outward side also bring the high absolute angular momentum inward to contribute effectively to TC intensity. By comparison, in CCAVE-EXP, the positive and negative agradient forces are detached at a relatively larger radius. Moreover, the magnitude of agradient force is much smaller than that in CVEX-EXP. As a result, the attenuated convergence is situated at a larger radius, which intensifies the vortex less effectively, and thus delays the vortex intensification.

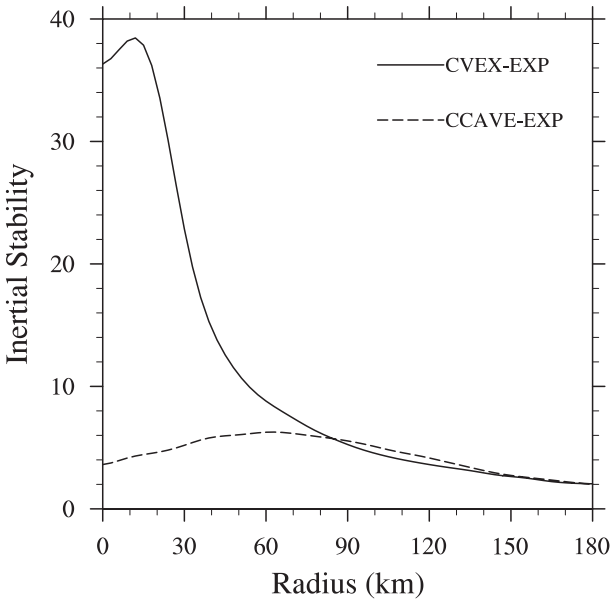

Fig. 6. Radial profile of the inertial stability parameter normalized by the local Coriolis parameter, averaged between 950 and 700 hPa during 24–48 h, in CVEX-EXP (sold line) and CCAVE-EXP (dashed line).

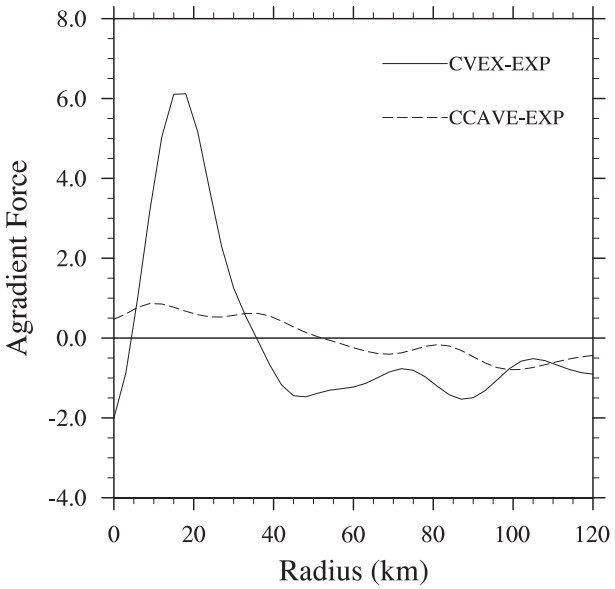

Fig. 7. Agradient force (units: m s^{-1} h^{-1}) averaged below 2 km, from 24 to 48 h, in CVEX-EXP (solid line) and CCAVE-EXP (dashed line).

4. Effect of the inner-core structure on TC track

In addition to the sensitivity of TC intensification to the different inner-core structures, the resulting structure also modulates the TC track. As demonstrated in Fig. 2b, during the first 36 h, both of the TCs have similar northwestward displacement, with a tiny difference in that the TC track in CVEX-EXP is located slightly to the east of that in CCAVE-

EXP. Interestingly, after 36 h of integration, the TC movement in CCAVE-EXP displays a more northward component than that in CVEX-EXP, and even makes a northeast turn during the period of 48–60 h. After 60 h, the TC translation in CCAVE-EXP shifts to the northwest, and then maintains an almost identical translation speed and direction to that in CVEX-EXP. Comparatively, the TC in CVEX-EXP sustains a basically uniform northwestward displacement. As a consequence, the TC track in CCAVE-EXP is displaced to the east of that in CVEX-EXP after 48 h. Therefore, the question naturally arises: what is responsible for the TC northeastward shift during the period from 36 to 60 h in CCAVE-EXP?

A TC on a β plane is primarily steered by the ventilation flow between β gyres in the absence of environmental flow. Therefore, the sudden change of TC track in CCAVE-EXP can be accounted for by the steering flow related to the ventilation flow. In this study, the steering flow is calculated as the mean vector averaged within a radius of 300 km from the TC center between 850 and 300 hPa. Figure 8 displays the wavenumber-1 wind and geopotential height averaged between 850 and 300 hPa from 36 to 60 h. In CVEX-EXP (Fig. 8a), the wavenumber-1 structure features a dipole-like pattern with a positive (negative) anomaly of geopotential height and an anticyclonic (cyclonic) gyre to the east-northeast (west-southwest) of the TC center, which is in good agreement with the results of previous studies (e.g., Fiorino and Elsberry, 1989; Wang and Holland, 1996a). As a result, the wavenumber-1 asymmetry exhibits northwest-oriented ventilation flow with steering flow of approximately 1.4 m s^{-1} that coincides with the TC movement, as shown in Fig. 2b.

In sharp contrast, the wavenumber-1 geopotential height in CCAVE-EXP clearly takes on the secondary gyres within a radius of 300 km, with a positive (negative) anomaly along with an anomalously anticyclonic (cyclonic) circulation to the southwest (northeast) of the TC center, which is embedded within the primary β gyres. It is this pair of secondary gyres that modifies the β effect and rotates the mean ventilation flow clockwise from northwest to northeast, steering the TC to move northeastward (Fig. 8b). After 60 h, accompanied by the TC intensification and axisymmetrization as described in section 3, the primary β gyres are dominant and then shift the TC translation from northeast to northwest. The initiation of the secondary gyres in CCAVE-EXP can be attributed to the asymmetric convection. As depicted in Figs. 3i and 4b and d, the strong convective vortices in CCAVE-EXP are mostly distributed between the radii of 60 and 120 km in the northeastern section of the TC, which can warm the local atmospheric column and lower the geopotential height by hydrostatic adjustment, such that the gyre structure is modified with an anomalously negative (positive) geopotential height to the northeast (southwest), centered at the radius of 90 km. After 60 h, the vortex in CCAVE-EXP intensifies and develops a more axisymmetric and vertically aligned structure. The decreased structural asymmetry, to a lesser extent, modifies the β effect such that the TC track is re-oriented northwestward, similar to that in CVEX-EXP afterward, as displayed in Fig. 2b.

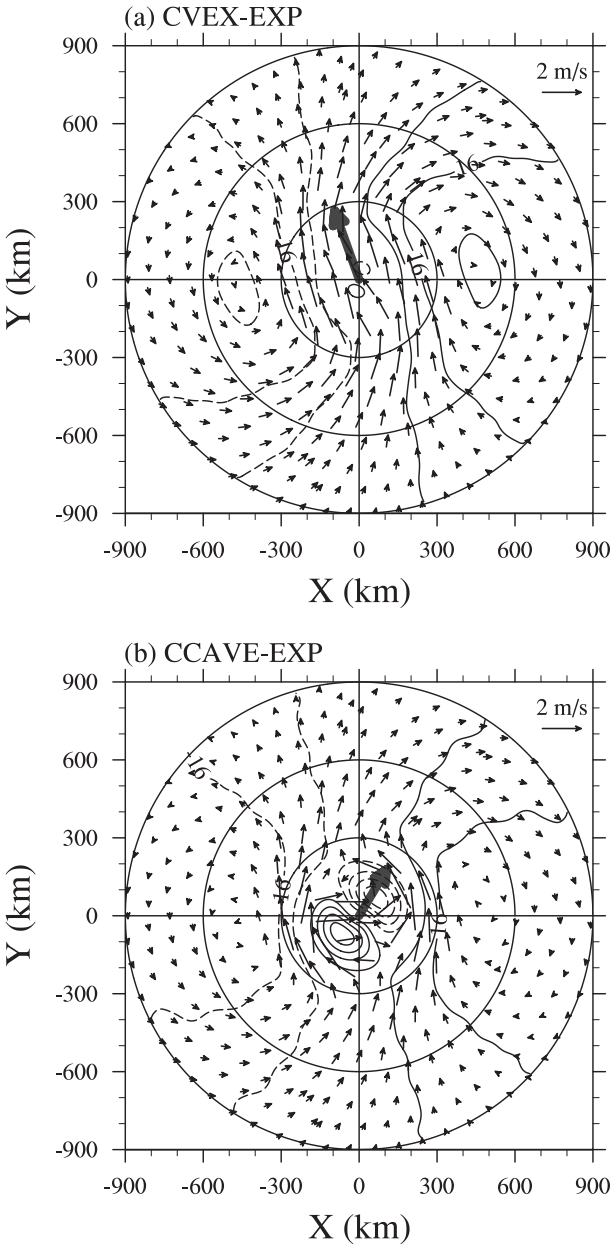

Fig. 8. The wavenumber-1 wind (vectors; units: m s^{-1}) and geopotential height (contours; units: m^2 s^{-2}) averaged between 850 and 300 hPa, from 36 to 60 h, in (a) CVEX-EXP and (b) CCAVE-EXP. The thick arrows indicate the direction and magnitude of steering flow, with a maximum value of 1.4 m s^{-1}. The domain shown in each panel is 1800 km × 1800 km. The *x*-axis and *y*-axis denote the east–west and south–north distance, respectively.

Previous studies have pointed out that a baroclinic TC tends to move to the region where the azimuthal wavenumber-1 component of (potential) vorticity tendency reaches a maximum (e.g., Holland, 1983; Wu and Wang, 2000). To further understand the role of the asymmetric structure in the TC track, the simulated wavenumber-1 component of the vorticity tendency averaged between 850 and 300 hPa from 36 to 60 h is displayed in Fig. 9. As seen in Fig. 9a, the

maximum vorticity tendency in CVEX-EXP is directed to the northwest, in alignment with the direction of TC movement and steering flow. The structure of the wavenumber-1 vorticity tendency is also consistent with the quasi-steady solution in streamfunction tendency analysis in Fiorino and Elsberry (1989). Similar to the structure in CCAVE-EXP as shown in Fig. 8b, the distribution of the wavenumber-1 vorticity tendency features a pair of northeast–southwest-oriented gyres within a radius of 300 km, with a positive (negative) anomaly to the northeast (northwest) of the TC center. As discussed above, the anomalously enhanced convective heating to the northeast acts as a major contributor to the local increasing of vorticity with time, favorable for the northeastward displacement of the TC during the spin-up period.

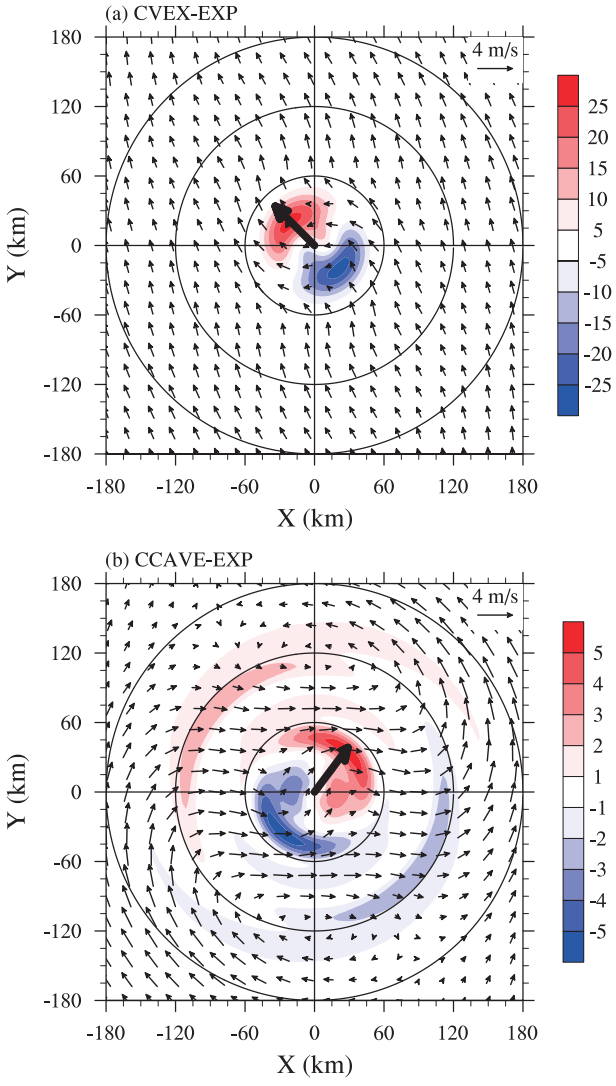

Fig. 9. The wavenumber-1 wind (vectors; units: m s^{-1}) and vorticity tendency (shaded; units: $\times 10^{-9}$ s^{-2}) averaged between 850 and 300 hPa, from 36 to 60 h, in (a) CVEX-EXP and (b) CCAVE-EXP. The thick arrows indicate the direction of maximum vorticity tendency. The domain shown in each panel is 360 km × 360 km. The *x*-axis and *y*-axis denote the east–west and south–north distance, respectively.

5. Conclusion

The sensitivity of TC intensification and track to the initial inner-core structure is investigated using the WRF model. The initial symmetric vortices with the same outer-core but different inner-core structures (convex- versus concave-shaped inner-core wind profiles) are specified on a β plane. It is found that the vortex with a convex-shaped inner-core wind profile in CVEX-EXP intensifies earlier than that in CCAVE-EXP, but has a similar intensification rate after the intensification is initiated. In the final steady state, the TC in CCAVE-EXP is observed to be somewhat weaker than its counterpart in CVEX-EXP, due to the more active outer rainband in CCAVE-EXP that can act as an inhibitor for TC intensification from the dynamic and thermodynamic perspectives.

In the early stage, the strong wind in the inner-core region in CVEX-EXP can trigger more surface heat flux, and then convective heating, within a radius of 60 km. Convectively generated small-scale vortices tend to aggregate rapidly in the region with strong ambient vorticity, and form a self-amplified vortex through a bottom-up development process. In contrast, the inner-core convection is less active in CCAVE-EXP, whereas most of the convective cells spread outside the inner-core region to the northeast of the TC center. The outer-core structural asymmetry in CCAVE-EXP can be ascribed to the β effect that generates a wind speed maximum to the northeast of the vortex. The well-defined low-level β skirt within a relatively small radius in CVEX-EXP can favor the formation of a well-organized convective band outside the eyewall, via the maintenance of long-lasting deep convection and the upscale transfer of energy from convective-scale motion, which accelerates TC intensification. Owing to the high inertial stability in the inner-core region in CVEX-EXP, the inner-core convective heating can effectively warm the atmospheric column and convert potential energy to kinetic energy. Besides, the striking PBL imbalance in CVEX-EXP in the early stage drives the significant convergence in conjunction with subgradient and supergradient flows, along with the radially inward transport of high angular momentum, assisting in the advancement of TC intensification. Although the TC in CCAVE-EXP has a delayed intensification, it also experiences a rapid intensification once the convective ring and the radius of maximum wind contract significantly in such a way that the efficiency with which the convective heating forces the secondary circulation becomes increased.

In terms of TC track, the vortex in CVEX-EXP sustains a consistent northwestward displacement during the simulation. In contrast, the TC in CCAVE-EXP experiences a northeastward recurvature during the period from 36 to 60 h, and afterward restores to the northwest direction as TC intensification and axisymmetrization proceed. Different from the larger-scale primary gyres due to the meridional gradient of planetary vorticity in CVEX-EXP, a pair of smaller-scale secondary gyres in CCAVE-EXP is embedded within the primary β gyres, consisting of a cyclonic one to the northeast and an anticyclonic one to the southwest. The combination of primary and second gyres in CCAVE-EXP modifies the

direction of ventilation flow, steering the TC to move northeastward when the asymmetric structure is significant. The northeast–southwest-oriented secondary gyres in CCAVE-EXP are closely related to the enhanced convective heating to the northeast of the TC center outside 60 km. As a consequence, the wavenumber-1 minimum geopotential height and maximum vorticity tendency correspond well with the TC translation direction.

Acknowledgements. This study was supported financially by the National Basic Research Program of China (Grant No. 2014CB953902) and the National Natural Science Foundation of China (Grant Nos. 41275001 and 41475074).

REFERENCES

Bui, H. H., R. K. Smith, M. T. Montgomery, and J. Y. Peng, 2009: Balanced and unbalanced aspects of tropical cyclone intensification. *Quart. J. Roy. Meteor. Soc.*, **135**, 1715–1731.

Chan, J. C. L., and R. T. Williams, 1987: Analytical and numerical studies of the beta-effect in tropical cyclone motion. Part I: Zero mean flow. *J. Atmos. Sci.*, **44**, 1257–1265.

DeMaria, M., 1985: Tropical cyclone motion in a nondivergent barotropic model. *Mon. Wea. Rev.*, **113**, 1199–1210.

DeMaria, M., 1996: The effect of vertical shear on tropical cyclone intensity change. *J. Atmos. Sci.*, **53**, 2076–2088.

DeMaria, M., and W. H. Schubert, 1984: Experiments with a spectral tropical cyclone model. *J. Atmos. Sci.*, **41**, 901–924.

Dudhia, J., 1989: Numerical study of convection observed during the winter monsoon experiment using a mesoscale two-dimensional model. *J. Atmos. Sci.*, **46**, 3077–3107.

Ebita, A., and Coauthors, 2011: The Japanese 55-year reanalysis "JRA-55": An interim report. *SOLA*, **7**, 149–152.

Emanuel, K., C. DesAutels, C. Holloway, and R. Korty, 2004: Environmental control of tropical cyclone intensity. *J. Atmos. Sci.*, **61**, 843–858.

Fang, J., and F. Q. Zhang, 2012: Effect of beta shear on simulated tropical cyclones. *Mon. Wea. Rev.*, **140**, 3327–3346.

Fiorino, M., and R. L. Elsberry, 1989: Some aspects of vortex structure related to tropical cyclone motion. *J. Atmos. Sci.*, **46**, 975–990.

Ge, X. Y., W. Xu, and S. W. Zhou, 2015: Sensitivity of tropical cyclone intensification to inner-core structure. *Adv. Atmos. Sci.*, **32**(10), 1407–1418, doi: 10.1007/s00376-015-4286-5.

Hack, J. J., and W. H. Schubert, 1986: Nonlinear response of atmospheric vortices to heating by organized cumulus convection. *J. Atmos. Sci.*, **43**, 1559–1573.

Holland, G. J., 1983: Tropical cyclone motion: Environmental interaction plus a beta effect. *J. Atmos. Sci.*, **40**, 328–342.

Hong, S.-Y., J. Dudhia, and S.-H. Chen, 2004: A revised approach to ice microphysical processes for the bulk parameterization of clouds and precipitation. *Mon. Wea. Rev.*, **132**, 103–120.

Huang, Y.-H., M. T. Montgomery, and C.-C. Wu, 2012: Concentric eyewall formation in Typhoon Sinlaku (2008). Part II: Axisymmetric dynamical processes. *J. Atmos. Sci.*, **69**, 662–674.

Li, T., X. Y. Ge, M. Peng, and W. Wang, 2012: Dependence of tropical cyclone intensification on the Coriolis parameter. *Tropical Cyclone Research and Review*, **1**, 242–253.

Madala, R. V., and S. A. Piacsek, 1975: Numerical simulation of asymmetric hurricanes on a β-plane with vertical shear. *Tellus*, **27**, 453–468.

Mlawer, E. J., S. J. Taubman, P. D. Brown, M. J. Iacono, and S. A. Clough, 1997: Radiative transfer for inhomogeneous atmospheres: RRTM, a validated correlated-k model for the longwave. *J. Geophys. Res.*, **102**, 16 663–16 682.

Noh, Y., W. G. Cheon, S. Y. Hong, and S. Raasch, 2003: Improvement of the K-profile model for the planetary boundary layer based on large eddy simulation data. *Bound.-Layer Meteor.*, **107**, 401–427.

Peng, M. S., B.-F. Jeng, and R. T. Williams, 1999: A numerical study on tropical cyclone intensification. Part I: Beta effect and mean flow effect. *J. Atmos. Sci.*, **56**, 1404–1423.

Powell, M. D., 1990: Boundary layer structure and dynamics in outer hurricane rainbands. Part II: Downdraft modification and mixed layer recovery. *Mon. Wea. Rev.*, **118**, 918–938.

Rappaport, E. N., and Coauthors, 2009: Advances and challenges at the National Hurricane Center. *Wea. Forecasting*, **24**, 395–419.

Schecter, D. A., and D. H. Dubin, 1999: Vortex motion driven by a background vorticity gradient. *Phys. Rev. Lett.*, **83**, 2191.

Schubert, W. H., and J. J. Hack, 1982: Inertial stability and tropical cyclone development. *J. Atmos. Sci.*, **39**, 1687–1697.

Shapiro, L. J., and H. E. Willoughby, 1982: The response of balanced hurricanes to local sources of heat and momentum. *J. Atmos. Sci.*, **39**, 378–394.

Terwey, W. D., and M. T. Montgomery, 2008: Secondary eyewall formation in two idealized, full-physics modeled hurricanes. *J. Geophys. Res.*, **113**, D12112, doi: 10.1029/2007JD008897.

Wang, Y. Q., 1995: An inverse balance equation in sigma coordinates for model initialization. *Mon. Wea. Rev.*, **123**, 482–488.

Wang, Y. Q., 2009: How do outer spiral rainbands affect tropical cyclone structure and intensity? *J. Atmos. Sci.*, **66**, 1250–1273.

Wang, Y. Q., and G. J. Holland, 1996a: The beta drift of baroclinic vortices. Part I: Adiabatic vortices. *J. Atmos. Sci.*, **53**, 411–427.

Wang, Y. Q., and G. J. Holland, 1996b: The beta drift of baroclinic vortices. Part II: Diabatic vortices. *J. Atmos. Sci.*, **53**, 3737–3756.

Wu, C.-C., and K. A. Emanuel, 1993: Interaction of a baroclinic vortex with background shear: Application to hurricane movement. *J. Atmos. Sci.*, **50**, 62–76.

Wu, L. G., and B. Wang, 2000: A potential vorticity tendency diagnostic approach for tropical cyclone motion. *Mon. Wea. Rev.*, **128**, 1899–1911.

Wu, L. G., and S. A. Braun, 2004: Effects of environmentally induced asymmetries on hurricane intensity: A numerical study. *J. Atmos. Sci.*, **61**, 3065–3081.

Zhu, T., and D.-L. Zhang, 2006: The impact of the storm-induced SST cooling on hurricane intensity. *Adv. Atmos. Sci.*, **23**, 14–22, doi: 10.1007/s00376-006-0002-9.